Fuel 345 (2023) 128181

Contents lists available at ScienceDirect

Fuel

journal homepage: www.elsevier.com/locate/fuel

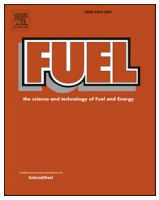

Full Length Article

Potential of iron-based composites derived from sucrose foam for mercury removal and safe recovery

L. López-Toyos, M.A. López-Antón *, E. Rodríguez, R. García, M.R. Martínez-Tarazona

Instituto de Ciencia y Tecnología del Carbono, INCAR-CSIC, C/Francisco Pintado Fe, 26, 33011 Oviedo, Spain

ARTICLE INFO

Keywords:
Mercury emission reduction
Sucrose carbon foam
Iron oxide nanoparticles
Coal-fired power plants

ABSTRACT

Although various methods for removal of elemental mercury from gas streams have been proposed, the control of mercury emissions to the environment from anthropogenic sources, mainly coal-fired power plants, remains unresolved in many countries worldwide. Meanwhile, the Minamata Convention and the IED of the European Commission continue to impose restrictions for its control and mitigation. In this work, a new material based on a sucrose foam impregnated with iron oxide nanoparticles has been developed for the adsorption of elemental mercury from flue gases allowing the regeneration of the material and the recovery of elemental mercury. Of the different iron oxides supported on the sucrose foam, αFe_2O_3 nanoneedles were found to be the most efficient in capturing mercury through a Mars-Maessen mechanism and the forming of HgO. The adsorbents developed proved to be effective in the presence of SO_2 and H_2O, with the O_2 present in the gas playing a key role in the regeneration of the material. From the results found sucrose foam-based αFe_2O_3 composite could be an attractive alternative to traditional non-regenerable activated carbons, reducing costs and being environmentally sustainable.

1. Introduction

Mercury is emitted from different natural and anthropogenic sources, travelling short or long distances depending on its chemical forms, to finally be locally and globally deposited. High levels of mercury exposure can produce harmful effects on the nervous, digestive and immune systems [1]. Therefore, mercury reduction is an essential step for a global environmental protection. This concern is reflected in the so-called Minamata Convention on Mercury, which came into force in 2017 [2]. All parties ratifying the Convention are required to control and reduce mercury emissions from the main anthropogenic sources (fossil fuel combustion, non-ferrous metal smelting, cement production, wastes incineration, etc). Although the Convention does not specify reduction amounts nor control technologies, several measures, such as the best available techniques (BAT) and multipollutant control technologies, are required. The necessary levels of reduction of mercury emissions from the main anthropogenic sources are included in a directive of the European Parliament [3] and in the US Environmental Protection Agency [4].

Mercury is a trace impurity in coal that, when burned, can be released into the environment. Although different economic and technological scenarios are contemplated by countries around the world, the global consumption of coal in the coal-fired power plants does not seem to decrease greatly during 2020–2030 [5–7]. Global coal consumption was estimated considering the development of power industry and clean energy production and the standard coal consumption for electric power production worldwide.

It is estimated that the distribution of mercury species in the total mercury emission to the air from power plants is: 87% elemental mercury (Hg^0), 5% oxidized mercury (Hg^{2+}) and 8% mercury bound to particulate matter (Hg_p) [8,9]. The removal of Hg^0 is the main unsolved concern.

The use of certain sorbents and catalysts that oxidize mercury is an efficient technology for the retention of Hg^0 from coal-fired power plants [10]. Many researchers have studied Hg^0 oxidation by several catalysts and different mechanisms have been proposed [11,12]. Nowadays, the highly volatile and water-insoluble Hg^0 is mostly reduced by activated carbon injection and selective catalytic reduction (SCR) coupled with flue gas desulphurization (FGD) units [13,14]. However, the injection of activated carbon can limit the use of fly ash in concrete production due to an increase in its carbon content [13,15]. The incorporation of magnetic materials (Fe_3O_4/γ-Fe_2O_3) in a sorbent

* Corresponding author.
E-mail address: marian@incar.csic.es (M.A. López-Antón).

https://doi.org/10.1016/j.fuel.2023.128181
Received 29 September 2022; Received in revised form 15 March 2023; Accepted 19 March 2023
Available online 28 March 2023

would allow the separation of the fly ashes by applying an external magnetic field [16,17]. Efficiencies close to 90% have been achieved using magnetic-based attapulgite sorbents depending on the gases present in the gas stream [18,19]. On the other hand, activated carbon injection has other drawbacks in terms of environmental protection, such as the regeneration process. Traditional sulfur- or halogen-impregnated activated carbons [20], in which Hg^0 is mainly retained through chemical adsorption, are not regenerable sorbents, leading to the generation of new mercury-contaminated waste after depletion.

The most studied regenerable sorbents to date are: 1) noble metals-based materials and 2) metal oxides-based materials [21–23]. Metals and metal oxides are deposited on supports with the appropriate physical, chemical and textural properties for an adequate dispersion of the additive, as well as for gas circulation. Activated carbons, carbon monoliths and carbon foams, among others, have been used as carbonaceous supports [24–26]. However, and taking into account the new environmental policies [27], the precursors used as supports for new carbon materials will have to be not only economically viable but also environmentally sustainable and remain within the framework of a circular economy. In many cases, this is not an easy task to accomplish.

Noble metals such as gold (Au), silver (Ag), and palladium (Pd) have the ability to amalgamate with Hg^0. A sorbent loaded with any of them, can be easily regenerated after use by heating, with the concomitant condensation and isolation of Hg^0 [28–30]. In order to reduce the costs associated with the use of noble metals, materials doped with metal oxides have also been developed as regenerable sorbents, most of them based on manganese oxides (MnOx) [31–33]. Recently, biochars doped with magnetite (Fe_3O_4) have been proven to be effective for the capture of Hg^0 in flue gas [34]. However, the possibility of regenerating the sorbent was not evaluated.

In order to solve some of the aforementioned drawbacks associated with the main sorbents used to date for Hg^0 removal, in this work, a new material based on carbon foam was developed. The carbon material was impregnated with iron oxides (FexOy) to improve the mercury adsorption capacity and to allow the regeneration of the sorbent. In addition, sucrose was used as a precursor for the carbon foam leading to an economically and environmentally sustainable sorbent. The iron-based sorbent derived from sucrose foam is developed with the intention of be regenerated and used in the flue gas stream at the end of the coal combustion cycle where most of Hg^{2+} may already have been retained, assuming that it will be used in a power plant in where DeNox, particles control and desulphurization devices are operating.

2. Materials and methods

2.1. Carbon foam preparation and characterization

A carbon foam (SF) was elaborated using commercial sucrose as precursor and $Fe(NO_3)_3\ 9H_2O$ (0.3% wt Fe) as foaming enhancer and activating agent. The first step to obtain the foam consists of the preparation of a caramel by heating sucrose up to 170 °C. After cooling, the caramel was placed in an oven with air circulation for the actual foaming process, which was performed in two successive steps: (i) heating up to 150 °C at 2 °C min^{-1} and (ii) heating up to 250 °C at 2 °C min^{-1}. The residence times at each temperature were 2.5 and 3 h, respectively. The resultant foam was carbonized for 2 h at 800 °C in a horizontal tubular furnace, under an argon flow of 50 mL min^{-1} and a heating rate of 5 °C min^{-1}.

Two impregnation methods, involving different thermal treatments, were used to obtain SFs loaded with different iron species: (A) $FeSO_4\ 7H_2O$ and CH_3COONa in water [35] and (B) $Fe(NO_3)_3\ 9H_2O$ in ethanol [36]. The resultant SFs were named according to the iron species present: SF-FeOOH (method A), SF-αFe_2O_3 (method A followed by thermal treatment at 300 °C), SF-FexOy (method B with carbonization at 500 °C) and SF-Fe-FexOy (method B with carbonization at 800 °C). At first, the SFs were loaded with 20 wt% Fe. Afterwards, the SF displaying higher mercury retention capacity was also loaded with 5, 10 and 30 wt% Fe, in order to evaluate the effect of iron concentration.

The distribution and morphology of the iron nanoparticles was studied by scanning electron microscopy (SEM), whereas the iron species were identified by X-ray diffraction (XRD).

The magnetic properties of the SFs were determined using a Microsense EV9 vibrating sample magnetometer (VSM), measuring the magnetization of the SF versus the magnetic field applied between 22 and –22 kOe at 300 K. The variation of the magnetization versus temperature was also determined for an applied magnetic field of 1 kOe.

The specific surface area of carbon foams was determined by the standard BET method using N_2 adsorption data. The total pore volume, V_t, was obtained from the amount of N_2 adsorbed at a relative pressure of 0.975, and the micropore volume, V_{micro}, was determined by fitting the Dubinin-Radushkevich (DR) equation to the N_2 adsorption isotherm. The mesopore volume, V_{meso}, was calculated as the difference between V_t and V_{micro}. The macroporous texture of the carbon foams was determined by Hg intrusion analysis performed on Micromeritics AutoPore IV apparatus, operating at a maximum pressure of 227 MPa. The samples were outgassed at 120 °C overnight before analysis.

The surface chemical composition of the SFs was investigated by X-ray photoelectron spectroscopy (XPS). XPS analyses were carried out on a Specs spectrometer, using MgKα (1253.6 eV) radiation from a double anode at 50 w. Binding energies for the high-resolution spectra were calibrated by setting C 1 s to 284.6 eV.

2.2. Experimental design

The mercury retention capacity of the carbon foam composites was evaluated in a fixed-bed reactor (Fig. 1), which is heated in a vertical furnace at 80 °C. The simulated flue gas consists of 15% CO_2, 6% O_2, 8% H_2O and 100 ppm SO_2 in N_2 (i.e., in an atmosphere relatively free of acid gases after SCR, ESP and FGD units). Elemental mercury (Hg^0) is incorporated into the gaseous stream from a commercial permeation tube, with a concentration of 100 μg m^{-3}. The Hg^0 in the gas phase that is not retained in the fixed-bed is registered in the VM-3000 analyzer. The oxidized mercury (Hg^{2+}) that is not retained in the sorbent is captured in an ionic exchanger resin (Dowex® 1x8), developed to selectively capture Hg^{2+} [37] and placed at the outlet of the fixed-bed. The Hg^{2+} captured in the resin was measured by using an automatic mercury analyser AMA 254. Once the adsorption cycle has finished, the sorbent is heated up to 450 °C at 2 °C min^{-1} in an inert N_2 atmosphere, to regenerate the carbon foam composite. After the Hg^0 adsorption–desorption cycle, Hg^0 is recovered by condensation and collected in a container [28] (Fig. 1), leaving the carbon foam composite free of Hg^0 and ready to be reused.

Possible mercury oxidation is also evaluated by temperature programmed desorption (HgTPD) by comparing the mercury desorption profile of the spent adsorbent with that obtained using a reference material (HgO). The desorption profiles are obtained by heating the sample at a rate of 50 °C min^{-1} under a N_2 flow of 500 mL min^{-1} [38].

3. Results and discussion

3.1. Characterization of carbon foam composites

The morphologies and microstructures of the SFs impregnated with 20 wt% Fe using different methods were first investigated by SEM. As shown in Fig. 2a, SF possesses an interconnected porous framework, which can serve as a support for the anchoring of iron oxides on the surface (Fig. 2b-f). All the SFs have a multimodal porosity, with pores ranging from micro/mesopores to macropores. The presence of macropores (Figure S1) can be beneficial for gas passing through, whereas micro/mesopores can increase mercury adsorption due to their larger contact area (Table 1). An enhanced BET surface area means more exposed actives sites available for mercury adsorption. Therefore, a

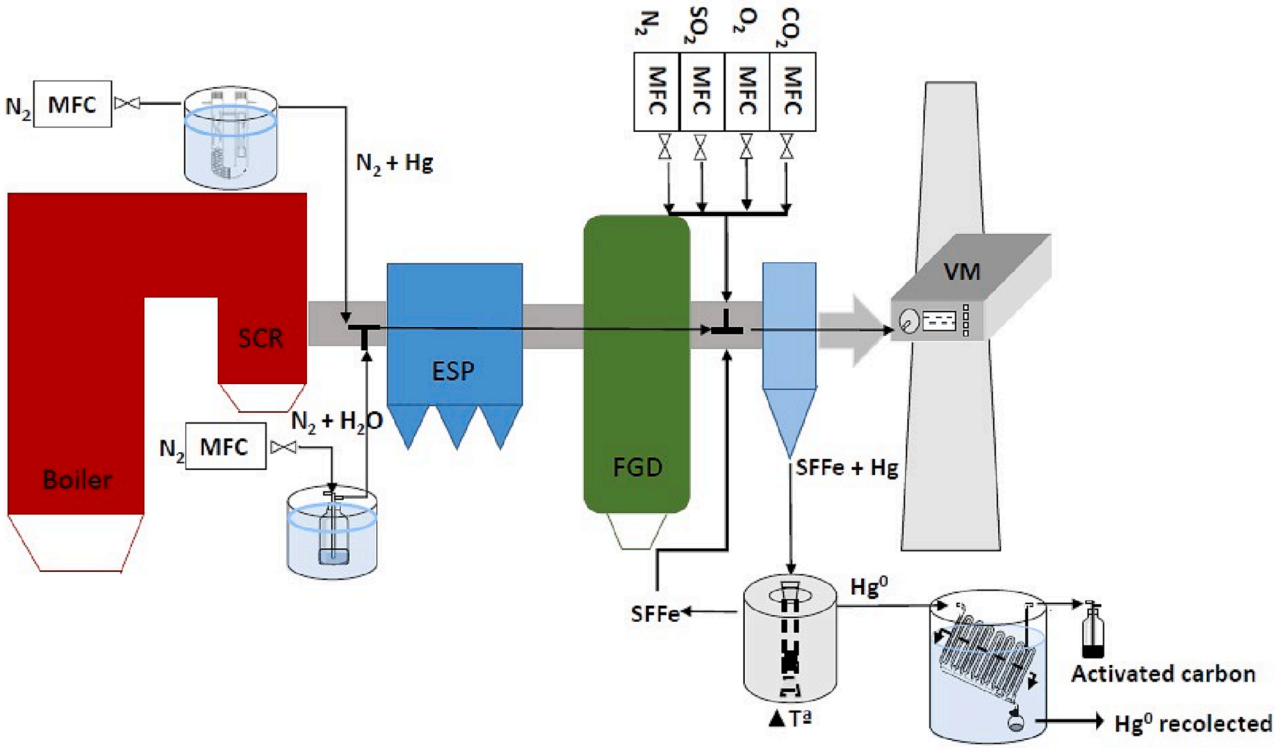

Fig. 1. Schematic diagram of the process for Hg^0 removal using SFs in coal combustion flue gases.

well- developed pore structure of sorbent will presumably favor mercury removal.

SF has a BET surface area of 306 $m^2\ g^{-1}$ and V_t of 0.24 $cm^3\ g^{-1}$, with a textural porosity composed of both micro and mesopores at similar ratios, 46 and 54%, respectively. The iron oxides/hydroxides are deposited coating the carbon structure of the foam (Fig. 2b-f), so it is expected that the composite foams show a reduction in their textural parameters. The results presented in Table 1 confirm slightly reductions in the BET surface area and the pore volume of the composites in comparison with the parent foam, being more pronounced in the sample impregnated with the method B and carbonized at 500 °C (SF-FexOy: 200 $m^2\ g^{-1}$ and 0.08 $cm^3\ g^{-1}$) (Table 1). In SEM image (Fig. 2e) is clearly visible, that iron oxide nanoparticles tend to agglomerate in sample SF-FexOy, which may lead to blockage of mayor number of pores. When the carbonization temperature was increased to 800 °C the agglomerates tend to disappear and the sample SF-Fe-FexOy showed comparable BET surface to those obtained by method A (Table 1).

As can be observed in Fig. 2b-f, the iron oxide/hydroxide nanoparticles are deposited in a wide range of morphologies, depending on the synthesis conditions (method and temperature). The method of oxidative hydrolysis with $FeSO_4\ 7H_2O$ and CH_3COONa in water favors the formation of nanoneedles (Fig. 2b-d), whereas the method with Fe $(NO_3)_3\ 9H_2O$ in ethanol promotes the formation of peanut-shaped nanoparticles (Fig. 2e-f). In addition, the iron species were different depending on the thermal treatment. The analysis by XRD (Fig. 3) revealed the presence of goethite in the sample synthetized by oxidative hydrolysis, along with other oxide phases, more specifically, oxides with spinel structure (magnetite or maghemite) (SF-FeOOH). The subsequent heat treatment of the sample at 300 °C caused a transformation of the iron oxide species into hematite (Fig. 3), although their original morphology of nanoneedles was preserved (SF-αFe_2O_3) (Fig. 2c-d). Nevertheless, the presence of magnetite and/or maghemite cannot be ruled out. In the detail of the SEM image at 5 μm (Fig. 2b) it can be observed that polyhedrons have also been formed. The iron species identified in the SFs impregnated with $Fe(NO_3)_3\ 9H_2O$ in ethanol were the iron oxides with spinel structure, magnetite and/or maghemite (SF-FexOy), with the presence of elemental iron when the temperature of carbonization increased from 500 to 800 °C (SF-Fe-FexOy).

A magnetic characterization was also carried out to confirm the presence of magnetite and/or maghemite in the samples. Fig. 4 shows the variation of magnetization versus temperature. A low-temperature phase transition is observed in the SFs. This corresponds to the Verwey transition, which is associated to magnetite. The presence of magnetite particles is more significant when the magnetization (emu/g) is higher (Figure S2). It must be taken into account that the presence of elemental iron also increases the saturation magnetization. This occurs in SF-Fe-FexOy (Figure S2), in which, elemental iron has already been identified by XRD (Fig. 3). The sample SF-FeOOH shows a higher hysteresis than SF-αFe_2O_3 (Figure S2), indicating a higher proportion of magnetite particles in SF-FeOOH. In Fig. 4, it can also be observed that sample SF-Fe-FexOy, unlike SF-FexOy, does not show a slight drop as the temperature increases. This behavior is characteristic when the material contains elemental iron. All these results agree with those found by XRD.

The results mentioned above reveal a successful synthesis of sucrose foam with different iron species incorporated into the carbon matrix with abundant active sites for the effective adsorption of mercury. The different morphology of the iron species on the SF surface can have a significant influence on the mercury adsorption performance and the subsequent regeneration of the sorbent.

3.2. *Effect of iron species on mercury adsorption*

Fig. 5 shows the mercury adsorption curves for the SFs. As explained in the previous section, the SFs contain different iron species depending on the impregnation method and the heat treatment. The curves represent the outlet/inlet Hg concentration ratio (C/C_0) versus time. The mercury adsorption capacities fell into the following increasing order: SF-FeOOH ≤ SF-Fe-FexOy < SF-FexOy < SF-αFe_2O_3, the later achieving an efficiency of 100% ($C/C_0 = 0$) and a mercury retention capacity of 90 ± 10 μg g^{-1}.

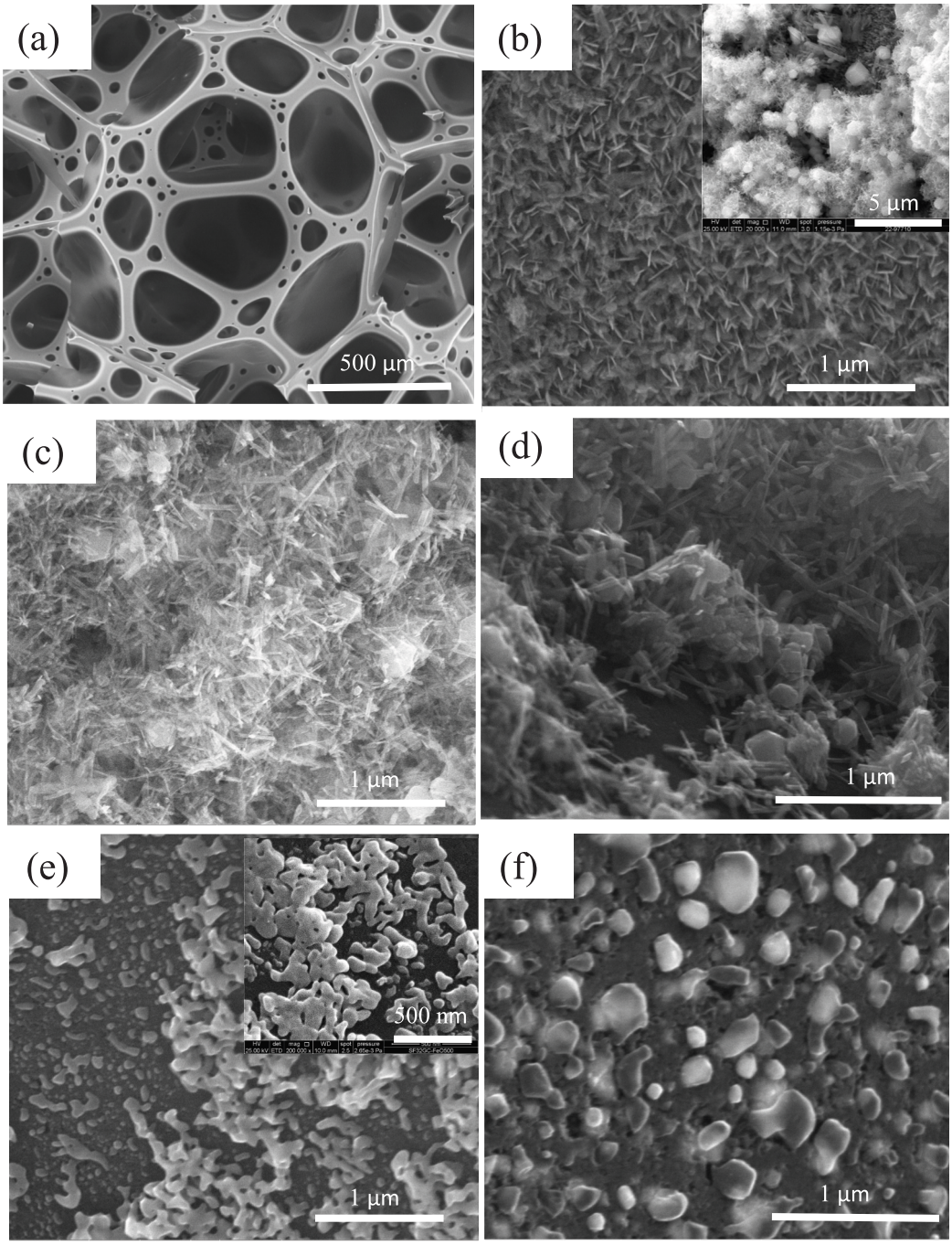

Fig. 2. SEM images of a) SF, b) SF-FeOOH, c) and d) SF-αFe_2O_3, e) SF-FexOy and f) SF-Fe-FexOy.

Table 1
Textural properties of the carbon foams.

	S_{BET} ($m^2\ g^{-1}$)	V_t ($cm^3\ g^{-1}$)	V_{micro} ($cm^3\ g^{-1}$)	V_{meso} ($cm^3\ g^{-1}$)
SF	306	0.24	0.13	0.11
SF-FeOOH	266	0.22	0.11	0.11
SF-αFe_2O_3	253	0.22	0.10	0.12
SF-FexOy	200	0.16	0.08	0.08
SF-Fe-FexOy	275	0.24	0.11	0.13

On the one hand, when the SFs impregnated with method A ($FeSO_4$ $7H_2O$ and CH_3COONa in water) are compared, the mercury retention capacity is much higher in SF-αFe_2O_3 than SF-FeOOH, displaying both the same iron morphology in the form of nanoneedles (Fig. 2b-d) and similar textural properties (Table 1). The outer layer of Fe^{3+} presents an empty orbital structure in the iron oxide (αFe_2O_3), which could be beneficial for the Fe/Hg^0 interaction [39]. On the other hand, when the SFs impregnated with method B ($Fe(NO_3)_3$ $9H_2O$ in ethanol) are compared, the SF treated at 800 °C resulting in the formation of elemental iron (SF-Fe-FexOy) shows a lower mercury retention capacity than the SF treated at 500 °C (SF-FexOy). Although the foam treated at a higher temperature has greater BET surface area and total pore volume (Table 1), the formation of elemental iron does not favour the retention

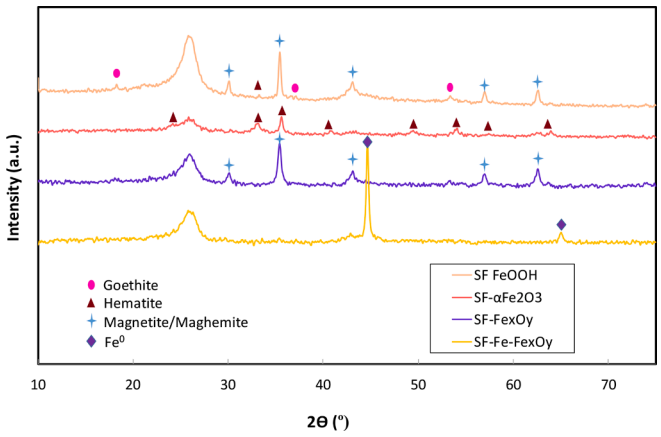

Fig. 3. XRD pattern of the resulting carbon foam composites SF-FeOOH, SF-αFe_2O_3, SF-FexOy and SF-Fe-FexOy.

of elemental mercury. In addition, the formation of the nanoparticles is less uniform in SF-Fe-FexOy (Fig. 2f).

These results suggest that: 1) the formation of αFe_2O_3 on the surface of the sucrose foam creates active sites for chemisorption/oxidization of the elemental mercury in the support (Fig. 5), and 2) a large number of needle-shaped nanoparticles with uniform size (Fig. 2c-d) improves the mercury adsorption as compared with peanut-shaped nanoparticles (Fig. 2 e-f).

3.3. Effect of iron concentration on mercury adsorption

The effect of iron concentration on mercury adsorption is examined through the comparative experiments in which the SF with the highest mercury retention (SF-αFe_2O_3) was impregnated with different iron amounts (5, 10, 20 and 30 %wt) (Fig. 6a). It must be taken into account that the Fe coating was not quantitative. The efficiency of the impregnation ranged between 40 and 70%, using 5–20% Fe, whereas the efficiency decreased to 25% for 30% Fe (Table S1).

The highest amount of iron deposited was reached using 20 wt% Fe (Table S1), which favoured the mercury retention as a consequence of the greater number of active sites on the sorbent surface. It is also remarkable that the sample SF-αFe_2O_3 30 wt% Fe, unlike SF-αFe_2O_3 20 wt% Fe, showed a proportion of polyhedrons (Fig. 6b) higher than that of nanoneedles (Fig. 2c-d). The different morphology can be attributed to different synthesis conditions (pH) [40]. Taking into account that both samples showed the same iron species, the results suggest that nanoneedles are more beneficial for the adsorption/oxidation of elemental mercury than polyhedrons (Fig. 5).

3.4. Adsorption-Desorption cicles: The role of O_2

It is well-known that the O_2 present in the flue gas may play a key role in the mercury adsorption and regeneration process [36]. The mercury retention capacity of SF-αFe_2O_3 with 20 wt% Fe was evaluated in the flue gas containing various concentrations of O_2. As can be observed in Fig. 7a, the mercury retention capacity was improved when the O_2 content in the flue gas increased from 6 to 16%. O_2 had a promotion effect on mercury removal over SF-αFe_2O_3, probably as a consequence of the generation of active oxygen species and the regeneration of the oxygen consumed on the carbon foam surface [41], which favours the adsorption and oxidation process of elemental mercury.

Fig. 7a also shows the mercury retention capacity of SF-αFe_2O_3 with

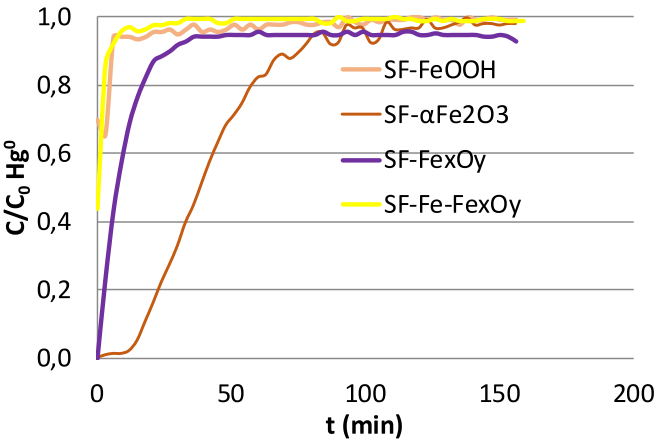

Fig. 5. Mercury adsorption curves of the SFs impregnated with 20 wt% Fe using $FeSO_4$ $7H_2O$ and CH_3COONa in water (SF-FeOOH and SF-αFe_2O_3) and Fe $(NO_3)_3$ $9H_2O$ in ethanol (SF-FexOy and SF-Fe-FexOy).

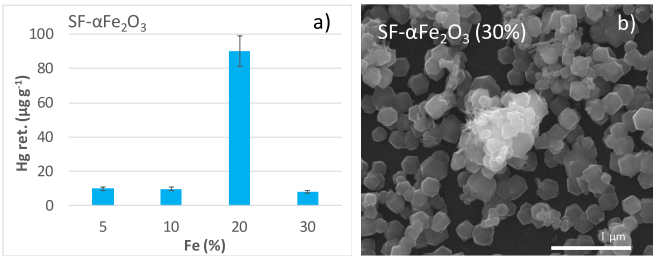

Fig. 6. (a) Mercury retention capacity of SF-αFe_2O_3 with 5, 10, 20 and 30 wt% Fe, and (b) SEM imagen of SF-αFe_2O_3 with 30 wt% Fe.

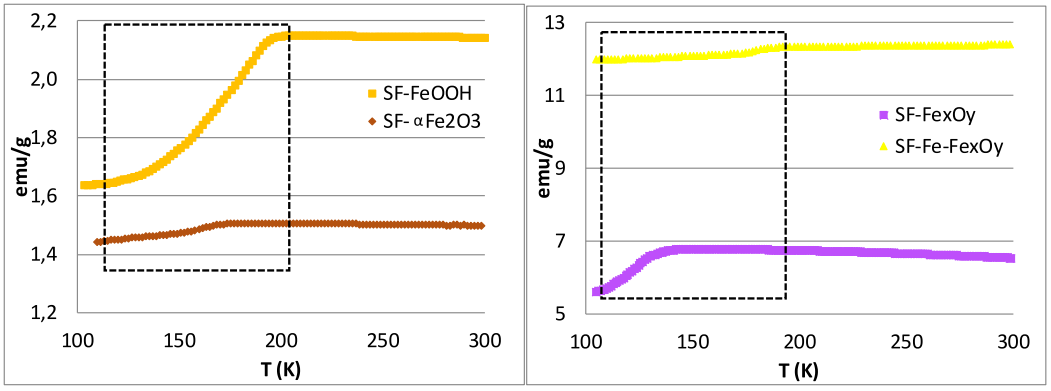

Fig. 4. Verwey transition of the resulting carbon foam composites impregnated with 20 wt% Fe using $FeSO_4$ $7H_2O$ and CH_3COONa in water (SF-FeOOH and SF-αFe_2O_3) and $Fe(NO_3)_3$ $9H_2O$ in ethanol (SF-FexOy and SF-Fe-FexOy).

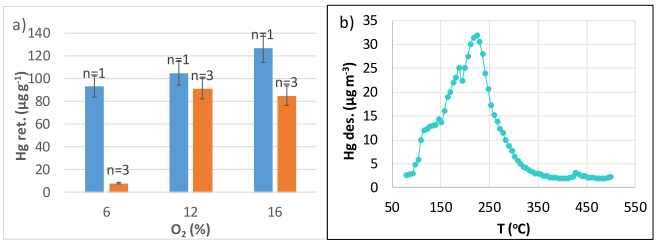

Fig. 7. (a) Mercury retention capacity of SF-αFe$_2$O$_3$ with 20 wt% Fe in cycles 1 and 3, and (b) mercury desorption curve.

20 wt% Fe after several cycles of adsorption–desorption with different concentration of O_2 in the flue gas. After the first adsorption cycle, the mercury retention capacity of SF-αFe$_2$O$_3$ decreased sharply with 6% O_2, suggesting that the hematite active sites were consumed during the retention experiments. However, the removal efficiency of the regenerated sucrose foams is still 67–90% when 12–16% O_2 is present in the flue gas after the third cycle. Therefore, the deactivation can be counteracted by adding O_2 to the gas stream to regenerate the sorbents.

These hypotheses were supported by XPS results. Fig. 8 shows the O 1 s and C 1 s core-level spectra of the fresh sorbent SF-αFe$_2$O$_3$ 20 wt% Fe, and after the second adsorption cycle (flue gas of 12% O_2). The C1s spectrum can be deconvoluted into three peaks at 533.1, 531.8 and 530.1 eV (Fig. 8a). The first peak at 533.1 eV corresponds to Si-O, which derived from the sand employed in the sorbent bed. In addition, this peak can be assigned to oxygen atoms in –O-C. The peak at 531.8 eV corresponds to O = C groups and also to chemisorbed oxygen in metal oxides. The peak at 530.1 eV lower binding energy is related to lattice oxygen in metal oxides groups [42,43]. As can be observed in Fig. 8a the lattice oxygen is reduced drastically after the adsorption cycle, thus its consumption may be related to the loss of mercury retention efficiency along cycles. By other hand, an increase of oxygen groups can be inferred from the C1s spectrum (Fig. 8b) after retention experiments. The fresh sorbent shows a main peak at 284.6 eV assigned to carbon group C-C and a little contribution from C-O (285.7 eV) and C-OOR groups (289.8 eV), whereas for the used sorbent an increase of these oxygen related peaks was observed. Therefore, the O_2 presence in the flue gas seems to promote creation of oxygen functionalities, which can be beneficial for mercury adsorption/oxidation reactions [44]. No significant differences were found in the Fe 2p spectra (Figure S3). The peaks at 709.5 and 710.8 eV were assigned to Fe^{2+} and Fe^{3+} ions, in agreement with XRD results. A satellite peak at 718.1 eV also corroborate the present of Fe^{3+} species (Figure S3).

It should also be taken into account that the GHSV in real conditions ranges between 2000 and 6000 h^{-1} [45], while in the experimental conditions of this study it is approximately 100000 h^{-1}. Therefore, the efficiency of mercury retention by the developed adsorbent would be improved, because a lower GHSV leads to higher residence times that favour mercury removal.

The mercury adsorbed on the spent SF-αFe$_2$O$_3$ was evaporated by thermal treatment at 450 °C in an N_2 atmosphere to subsequently reuse the adsorbent (Fig. 7b). The highest peak of mercury desorption occurs at approximately 225 °C, a remarkable result for sorbent regeneration at such low temperature. A low activation energy in the desorption process could be profitable for regeneration.

From this perspective and considering that SF-αFe$_2$O$_3$ showed good resistance to SO_2 and H_2O, which can compete with elemental mercury for active sites and lead to sorbent deactivation, αFe$_2$O$_3$-based sucrose foams could be an attractive alternative to traditional non-regenerable activated carbons, reducing costs and being environmentally sustainable.

3.5. Mechanism of mercury adsorption

Several studies have already shown that FexOy on carbon surface could supply lattice oxygen for elemental mercury adsorption and oxidation [36,46,47]. The elemental mercury removal could be explained by the Mars–Maessen mechanism, which is described by the following reactions [48]:

$$Hg(g) + SF \rightarrow Hg(ads) \quad (1)$$

$$Hg(ads) + \alpha Fe_2O_3 \rightarrow HgO(ads) + 2FeO \quad (2)$$

$$HgO(ads) + 2FeO + ½\ O_2 \rightarrow HgO(ads) + Fe_2O_3 \quad (3)$$

$$HgO(ads) + Fe_2O_3 \rightarrow HgFe_2O_4 \quad (4)$$

The first step is a physisorption process in which elemental mercury is adsorbed on the surface of the sucrose foam with a BET surface area of 253 $m^2\ g^{-1}$ (Table 1) (I). The second step is the reaction between the adsorbed mercury with hematite to oxidize mercury, by combination with chemisorbed oxygen and lattice oxygen, and reduce the sucrose foam surface (II). The adsorbent is then reoxidized by the oxygen present in the flue gas regenerating the consumed chemisorbed oxygen and lattice oxygen (III) and the binary oxide is finally formed (IV).

The formation of oxidized mercury is confirmed by the analysis of the mercury captured in the Dowex resin at the gas outlet of the fixed-bed. The percentage of oxidized mercury retained in the resin ranged between 15 and 20% of the total amount of elemental mercury that passed through the adsorbent. The results of HgTPD also suggest the formation and retention of oxidized mercury by the material developed here (Figure S4). The thermal desorption profile of commercial HgO that appears at 200–350 °C (Figure S4) can be associated with that obtained for the mercury retained in the spent adsorbent (Fig. 7b), both showing similar decomposition temperatures.

4. Conclusions

In this study, a cost-effective and environmentally sustainable adsorbent was developed for the capture of elemental mercury from flue gases. The adequate porous structure of the sucrose foam allowed the impregnation of different iron species with different morphology. The results showed that the αFe$_2$O$_3$ nanoneedles supported on the sucrose foam were the main active sites for the removal of elemental mercury. The sorbent proved to be effective in the presence of SO_2 and H_2O, being able to be regenerated by heating to 300 °C. The results of mercury speciation confirmed that mercury is retained in the form of HgO through a Mars-Maessen mechanism. The promising results lead to evaluating the efficiency of the adsorbent under real fuel gas conditions in the next step. In addition, the results found using commercial sucrose to synthesize the mercury adsorbent could provide a path for the utilization of waste from the agricultural industry.

CRediT authorship contribution statement

L. López-Toyos: Conceptualization, Investigation. **M.A. López-Antón:** Writing – original draft, Supervision, Project administration, Funding acquisition. **E. Rodríguez:** Investigation, Supervision. **R. García:** Writing – review & editing. **M.R. Martínez-Tarazona:** Writing – review & editing, Funding acquisition.

Declaration of Competing Interest

The authors declare that they have no known competing financial interests or personal relationships that could have appeared to influence the work reported in this paper.

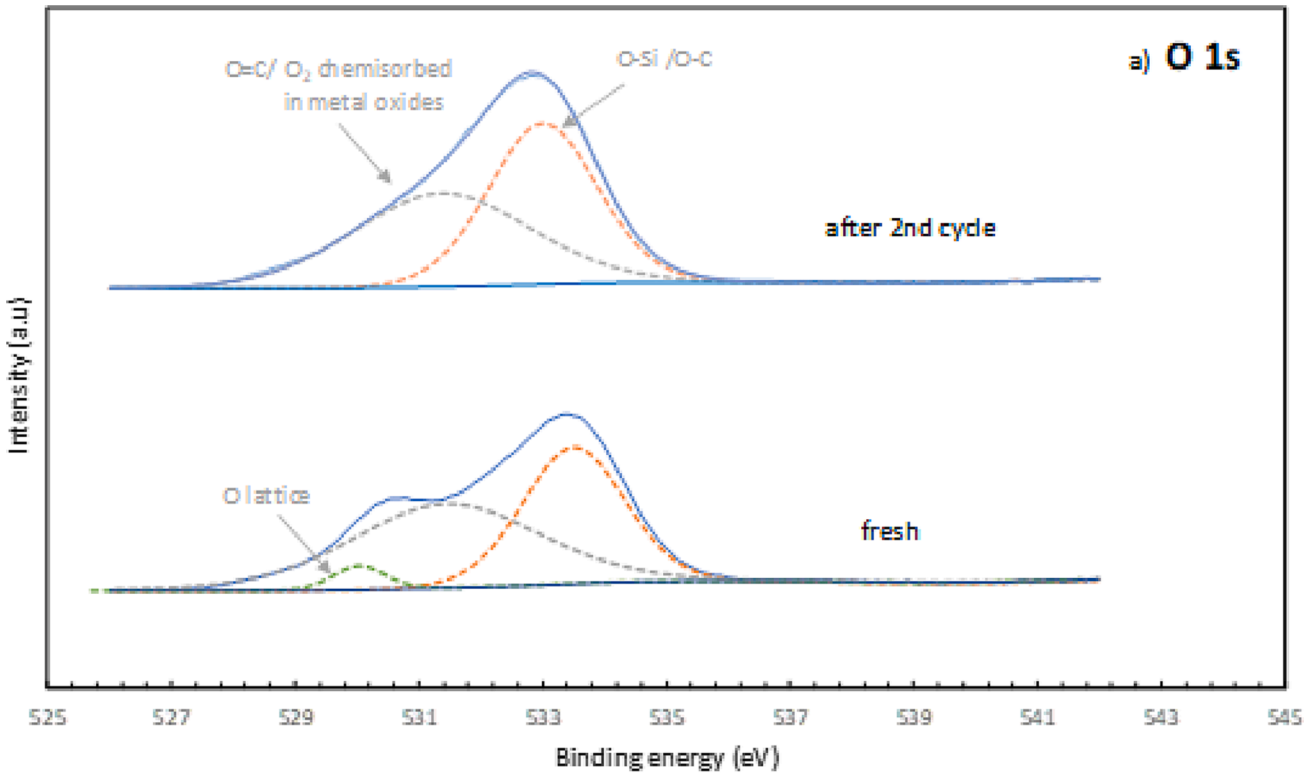

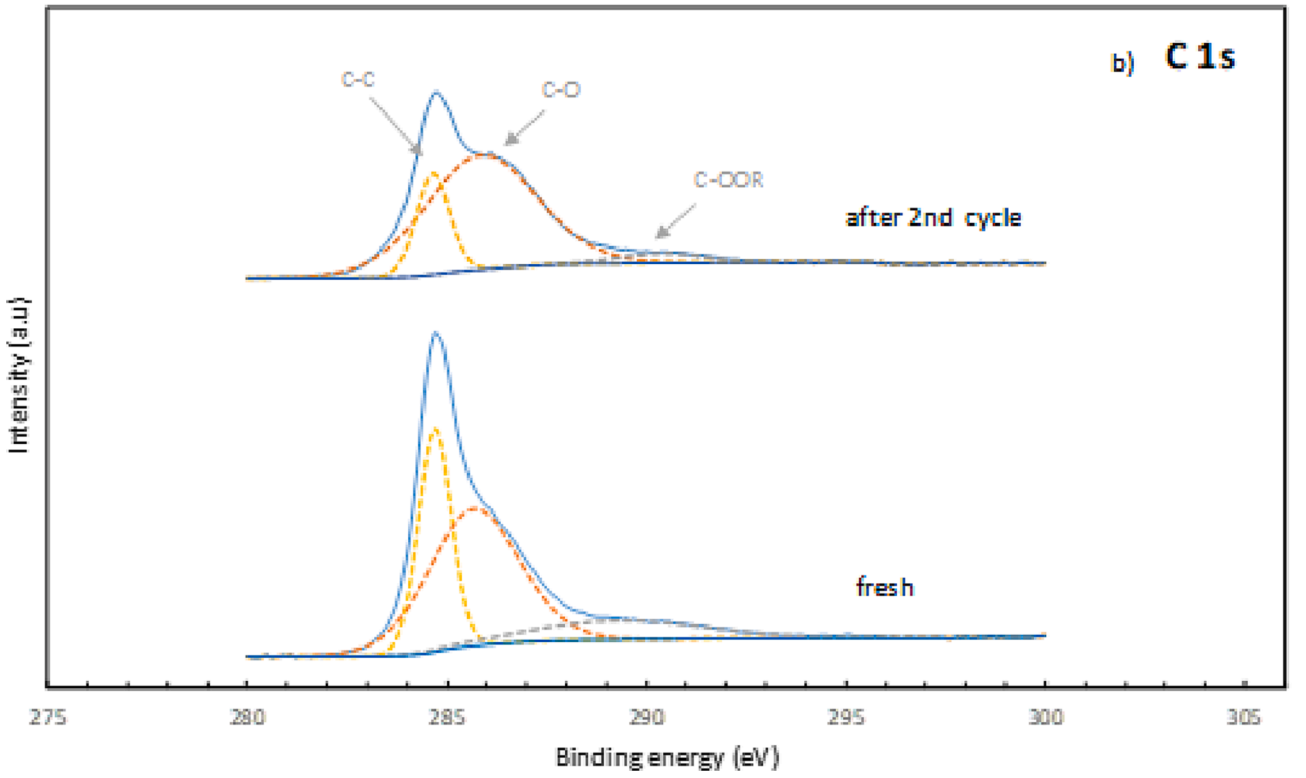

Fig. 8. A) o 1 s and b) C1s core level spectra for the fresh sorbent SF-αFe_2O_3 20 wt% Fe and after the second adsorption cycle carried out with 12% O_2.

Data availability

Data will be made available on request.

Acknowledgments

This work was funded by the research projects PID2020-113558RB-C43 (MCIN/ AEI/10.13039/501100011033) and IDI/2021/000031. The authors acknowledge the Spanish Research Council (CSIC) for the JAE-Intro fellowship awarded to Lucía López-Toyos (Ref: JAEICU21-INCAR-27).

Appendix A. Supplementary data

Supplementary data to this article can be found online at https://doi.org/10.1016/j.fuel.2023.128181.

References

[1] WHO. Mercury and health n.d. https://www.who.int/news-room/fact-sheets/detail/mercury-and-health (accessed September 29, 2022).
[2] UNEP. United Nations Environment Programme, 2017. Minamata Convention on Mercury, 2017. 2017.
[3] European Union directive 2021/2326 of 30 N 2021. EUR-Lex - 32021D2326 - EN - EUR-Lex 2021. https://eur-lex.europa.eu/legal-content/EN/TXT/?uri=CELEX:32021D2326 (accessed August 24, 2022).
[4] USEPA. Regulatory Actions - Final Mercury and Air Toxics Standards (MATS) for Power Plants | US EPA 2020. https://www.epa.gov/mats/regulatory-actions-final-mercury-and-air-toxics-standards-mats-power-plants (accessed August 24, 2022).
[5] Wu Q, Li G, Wang S, Liu K, Hao J. Mitigation Options of Atmospheric Hg Emissions in China. Environ Sci Technol 2018;52:12368–75. https://doi.org/10.1021/ACS.EST.8B03702.
[6] Wu Q, Wang S, Liu K, Li G, Hao J. Emission-Limit-Oriented Strategy To Control Atmospheric Mercury Emissions in Coal-Fired Power Plants toward the Implementation of the Minamata Convention. Environ Sci Technol 2018;52:11087–93. https://doi.org/10.1021/ACS.EST.8B02250.
[7] Wiatros-Motyka M. NOx control for high-ash coal-fired power plants in India. Clean Energy 2019;3:24–33. https://doi.org/10.1093/CE/ZKY018.
[8] Jensen RR, Karki S, Salehfar H. Artificial neural network-based estimation of mercury speciation in combustion flue gases. Fuel Process Technol 2004;85:451–62. https://doi.org/10.1016/J.FUPROC.2003.11.020.
[9] Burmistrz P, Kogut K, Marczak M, Zwoździak J. Lignites and subbituminous coals combustion in Polish power plants as a source of anthropogenic mercury emission. Fuel Process Technol 2016;152:250–8. https://doi.org/10.1016/J.FUPROC.2016.06.011.
[10] Pavlish JH, Hamre LL, Zhuang Y. Mercury control technologies for coal combustion and gasification systems. Fuel 2010;89:838–47. https://doi.org/10.1016/J.FUEL.2009.05.021.
[11] Liu X, Gao Z, Wang C, Zhao M, Ding X, Yang W, et al. Hg0 oxidation and SO3, Pb0, PbO, PbCl2 and As2O3 adsorption by graphene-based bimetallic catalyst ((Fe, Co)@N-GN): A DFT study. Appl Surf Sci 2019;496:143686. https://doi.org/10.1016/J.APSUSC.2019.143686.
[12] Yang W, Linlin L, Zhao M, Huang H, Ding X, Wu C, et al. Theoretical prediction of graphene-based single-atom iron as a novel catalyst for catalytic oxidation of Hg0 by O2. Appl Surf Sci 2020;508:145035. https://doi.org/10.1016/J.APSUSC.2019.145035.
[13] Sjostrom S, Durham M, Bustard CJ, Martin C. Activated carbon injection for mercury control: Overview. Fuel 2010;89:1320–2. https://doi.org/10.1016/J.FUEL.2009.11.016.
[14] Zhao S, Pudasainee D, Duan Y, Gupta R, Liu M, Lu J. A review on mercury in coal combustion process: Content and occurrence forms in coal, transformation, sampling methods, emission and control technologies. Prog Energy Combust Sci 2019;73:26–64. https://doi.org/10.1016/J.PECS.2019.02.001.
[15] Pflughoeft-Hassett DF, Hassett DJ, Buckley TD, Heebink LV, Pavlish JH. Activated carbon for mercury control: Implications for fly ash management. Fuel Process Technol 2009;90:1430–4. https://doi.org/10.1016/j.fuproc.2009.07.008.
[16] Chen Y, Guo X, Wu F. Development and evaluation of magnetic iron-carbon sorbents for mercury removal in coal combustion flue gas. J Energy Inst 2020;93:1615–23. https://doi.org/10.1016/J.JOEI.2020.01.023.
[17] Yang J, Zhao Y, Liang S, Zhang S, Ma S, Li H, et al. Magnetic iron–manganese binary oxide supported on carbon nanofiber (Fe3−xMnxO4/CNF) for efficient removal of Hg0 from coal combustion flue gas. Chem Eng J 2018;334:216–24. https://doi.org/10.1016/J.CEJ.2017.10.004.
[18] Dong L, Wang H, Huang Y, Zha J, Cheng H, Liu L, et al. γ-Fe2O3 decorated attapulgite composite modified with CuCl2 as magnetically separable sorbents for Hg0 removal from coal combustion flue gas. Chem Eng J 2021;408:127888. https://doi.org/10.1016/J.CEJ.2020.127888.
[19] Dong L, Wang H, Huang Y, Chen H, Cheng H, Liu L, et al. Elemental mercury removal from coal-fired flue gas using recyclable magnetic Mn-Fe based attapulgite sorbent. Chem Eng J 2021;407:127182. https://doi.org/10.1016/J.CEJ.2020.127182.
[20] Lopez-Antón MA, Tascón JM, Martínez-Tarazona MR. Retention of mercury in activated carbons in coal combustion and gasification flue gases. Fuel Process Technol 2002;77–78:353–8. https://doi.org/10.1016/S0378-3820(02)00054-1.
[21] Liu Y, Bisson TM, Yang H, Xu Z. Recent developments in novel sorbents for flue gas clean up. Fuel Process Technol 2010;91:1175–97. https://doi.org/10.1016/J.FUPROC.2010.04.015.
[22] Liu Y, Kelly DJA, Yang H, Lin CCH, Kuznicki SM, Xu Z. Novel Regenerable Sorbent for Mercury Capture from Flue Gases of Coal-Fired Power Plant. Environ Sci Technol 2008;42:6205–10. https://doi.org/10.1021/es800532b.
[23] Lopez-Anton MA, Fernández-Miranda N, Martínez-Tarazona MR. The application of regenerable sorbents for mercury capture in gas phase. Environ Sci Pollut Res 2016;23:24495–503. https://doi.org/10.1007/s11356-016-7534-z.
[24] Trobajo JR, Antuña-Nieto C, Rodríguez E, García R, López-Antón MA, Martínez-Tarazona MR. Carbon-based sorbents impregnated with iron oxides for removing mercury in energy generation processes. Energy 2018;159:648–55. https://doi.org/10.1016/j.energy.2018.06.189.
[25] Izquierdo MT, Ballestero D, Juan R, García-Díez E, Rubio B, Ruiz C, et al. Tail-end Hg capture on Au/carbon-monolith regenerable sorbents. J Hazard Mater 2011;193:304–10. https://doi.org/10.1016/J.JHAZMAT.2011.07.065.
[26] Antuña-Nieto C, Rodríguez E, Lopez-Anton MA, García R, Martínez-Tarazona MR. A candidate material for mercury control in energy production processes: Carbon foams loaded with gold. Energy 2018;159:630–7. https://doi.org/10.1016/j.energy.2018.06.172.
[27] European Commission. European Green Deal 2021. https://ec.europa.eu/clima/eu-action/european-green-deal_en (accessed August 24, 2022).
[28] Rodríguez-Pérez J, López-Antón MA, Díaz-Somoano M, García R, Martínez-Tarazona MR. Regenerable sorbents for mercury capture in simulated coal combustion flue gas. J Hazard Mater 2013;260:869–77. https://doi.org/10.1016/J.JHAZMAT.2013.06.026.
[29] Munson CL, Ramezan M, Granite E, Tennant J. Evaluation of Palladium-Based Sorbents for Trace Mercury Removal in Electricity Generation. Int J Clean Coal Energy 2014;3:65–76. https://doi.org/10.4236/ijcce.2014.34007.
[30] Cao T, Li Z, Xiong Y, Yang Y, Xu S, Bisson T, et al. Silica-Silver Nanocomposites as Regenerable Sorbents for Hg 0 Removal from Flue Gases. Environ Sci Technol 2017;51:11909–17. https://doi.org/10.1021/ACS.EST.7B01701.
[31] Scala F, Anacleria C, Cimino S. Characterization of a regenerable sorbent for high temperature elemental mercury capture from flue gas. Fuel 2013;108:13–8. https://doi.org/10.1016/j.fuel.2010.12.028.
[32] Cimino S, Scala F. Removal of Elemental Mercury by MnOx Catalysts Supported on TiO2 or Al2O3. Ind Eng Chem Res 2016;55:5133–8. https://doi.org/10.1021/ACS.IECR.5B04147/ASSET/IMAGES/LARGE/IE-2015-04147Z_0007.JPEG.
[33] Xu H, Qu Z, Zong C, Huang W, Quan F, Yan N. MnOx/graphene for the catalytic oxidation and adsorption of elemental mercury. Environ Sci Technol 2015;49:6823–30. https://doi.org/10.1021/ES505978N/SUPPL_FILE/ES505978N_SI_001.PDF.
[34] Yang J, Zhao Y, Ma S, Zhu B, Zhang J, Zheng C. Mercury Removal by Magnetic Biochar Derived from Simultaneous Activation and Magnetization of Sawdust. Environ Sci Technol 2016;50:12040–7. https://doi.org/10.1021/ACS.EST.6B03743.
[35] Janeiro-Tato I, Lopez-Anton MA, Baragaño D, Antuña-Nieto C, Rodríguez E, Peláez AI, et al. Immobilization of mercury in contaminated soils through the use of new carbon foam amendments. Environ Sci Eur 2021:33. https://doi.org/10.1186/S12302-021-00569-W.
[36] Antuña-Nieto C, Rodríguez E, López-Antón MA, García R, Martínez-Tarazona MR. Carbon materials loaded with maghemite as regenerable sorbents for gaseous Hg^0 removal. Chem Eng J 2020:387. https://doi.org/10.1016/j.cej.2020.124151.
[37] Fuente-Cuesta A, Diaz-Somoano M, Lopez-Anton MA, Martinez-Tarazona MR. Oxidised mercury determination from combustion gases using an ionic exchanger. Fuel 2014;122:218–22. https://doi.org/10.1016/J.FUEL.2014.01.030.
[38] Rumayor M, Lopez-Anton MA, Díaz-Somoano M, Martínez-Tarazona MR. A new approach to mercury speciation in solids using a thermal desorption technique. Fuel 2015;160:525–30. https://doi.org/10.1016/j.fuel.2015.08.028.
[39] Dong L, Huang Y, Chen H, Liu L, Liu C, Xu L, et al. Magnetic γ-Fe2O3-Loaded Attapulgite Sorbent for Hg0 Removal in Coal-Fired Flue Gas. Energy Fuel 2019;33:7522–33. https://doi.org/10.1021/ACS.ENERGYFUELS.9B01136/ASSET/IMAGES/LARGE/EF-2019-01136T_0015.JPEG.
[40] Cornell RM, Schwertmann U. The Iron Oxides Iron Oxides 2003. https://doi.org/10.1002/3527602097.
[41] Zhou Z, Liu X, Zhao B, Shao H, Xu Y, Xu M. Elemental mercury oxidation over manganese-based perovskite-type catalyst at low temperature. Chem Eng J 2016;288:701–10. https://doi.org/10.1016/J.CEJ.2015.12.057.
[42] Sevilla M, Fuertes AB. Chemical and structural properties of carbonaceous products obtained by hydrothermal carbonization of saccharides. Chemistry 2009;15:4195–203. https://doi.org/10.1002/CHEM.200802097.
[43] Huang WJ, Xu HM, Qu Z, Zhao SJ, Chen WM, Yan NQ. Significance of Fe2O3 modified SCR catalyst for gas-phase elemental mercury oxidation in coal-fired flue gas. Fuel Process Technol 2016;149:23–8. https://doi.org/10.1016/J.FUPROC.2016.04.007.
[44] Xu Y, Luo G, He S, Deng F, Pang Q, Xu Y, et al. Efficient removal of elemental mercury by magnetic chlorinated biochars derived from co-pyrolysis of Fe(NO3)3-laden wood and polyvinyl chloride waste. Fuel 2019;239:982–90. https://doi.org/10.1016/J.FUEL.2018.11.102.
[45] Yang J, Zhao Y, Guo X, Li H, Zhang J, Zheng C. Removal of elemental mercury from flue gas by recyclable CuCl2 modified magnetospheres from fly ash. Part 4.

Performance of sorbent injection in an entrained flow reactor system. Fuel 2018; 220:403–11. https://doi.org/10.1016/J.FUEL.2018.01.132.
[46] Yang W, Chen H, Han X, Ding S, Shan Y, Liu Y. Preparation of magnetic Co-Fe modified porous carbon from agricultural wastes by microwave and steam activation for mercury removal. J Hazard Mater 2020;381:120981. https://doi.org/10.1016/J.JHAZMAT.2019.120981.
[47] Ma Y, Mu B, Zhang X, Xu H, Qu Z, Gao L, et al. Ag-Fe3O4@rGO ternary magnetic adsorbent for gaseous elemental mercury removal from coal-fired flue gas. Fuel 2019;239:579–86. https://doi.org/10.1016/J.FUEL.2018.11.065.
[48] Granite EJ, Pennline HW, Hargis RA. Novel sorbents for mercury removal from flue gas. Ind Eng Chem Res 2000;39:1020–9. https://doi.org/10.1021/ie990758v.